Korean J. Chem. Eng., 38(3), 531-539 (2021)
DOI: 10.1007/s11814-020-0727-7

pISSN: 0256-1115
eISSN: 1975-7220

Decolorization of triarylmethane dyes, malachite green, and crystal violet, by sewage sludge biochar: Isotherm, kinetics, and adsorption mechanism comparison

Divine Damertey Sewu*,, Dae Sung Lee***, Seung Han Woo*,**,†, and Dimitrios Kalderis****

*Life Green Technology Co. Ltd., 875 Yuseong-daero, Yuseong-gu, Daejeon 34158, Korea
**Department of Chemical and Biological Engineering, Hanbat National University, 125 Dongseo-daero, Yuseong-gu, Daejeon 34158, Korea
***Department of Environmental Engineering, Kyungpook National University, 80 Daehak-ro, Buk-gu, Daegu 41566, Korea
****Department of Electronics Engineering, School of Engineering, Hellenic Mediterranean University, Chania, Crete, Greece
(*Received 8 September 2020 • Revised 24 November 2020 • Accepted 11 December 2020*)

Abstract−Sewage sludge biochar (SBC) was used as adsorbent to study the adsorption behavior of triarylmethane dyes, malachite green (MG; diaminotriphenylmethane), and crystal violet (CV; triaminotriphenylmethane). SBC exhibited high content (g/kg) of Al (65.8), P (64.6), Ca (57.3), and Fe (44.6). The Langmuir model showed that the affinity of MG for the surface of SBC was 22.6-times that of CV's (K_L=0.0053 l/mg); maximum Langmuir monolayer adsorption capacity of 69.5 mg/g for MG and 49.0 mg/g for CV. Similar functional groups and adsorption mechanisms like hydrogen bonding, π-π interaction, electrostatic interactions, and ion exchanges governed both MG and CV adsorption onto SBC. Both physisorption and chemisorption were involved in both dyes' adsorption (Redlich-Peterson model: R^2> 0.900) Leachability tests showed a dependency of leached metallic ions on the type of dye employed, where ion exchange was dominated by P, Al, Ca, K for MG, and Na, K, Ca for CV. Interestingly, although minimal, the stand-alone contribution of biochar-free ions on MG and CV decolorization was, respectively, 13% and 7.7% (Fe), 6.7% and 2.3% (K), 2.9% and 0% (Ca), and 0% and 0.8% (Mg), which showed that some adsorption-unrelated mechanism may have also contributed to decolorization of CV and MG.

Keywords: Adsorption Mechanism, Leaching, Sewage Sludge Biochar, Triarylmethane Dye, Waste

INTRODUCTION

Dyes find the most application in the textile industry, accounting for the release of 100 tons/year of effluent dye discharge into the environment [1]. They can be classified based on their chemical structure, color, application, or particle charge in solution; refer to [2] for more details. Based on the chemical structure, dyes can be classified as anthraquinone, thiazine, azo, triarylmethane, and many others [2], with triarylmethane – also belonging to the basic class – and diazo class noted as harboring higher rates of toxicity with median lethal doses (LD_{50}) greater than 2×10^3 mg/kg [3]. Triarylmethane dyes, in particular, are commonly used and account for about 30%-40% of the total dyes consumed by the textile industry [4]. They possess very high tinctorial value, such that obvious coloration is seen at concentrations less than 1 ppm [5]. It is, therefore, necessary to rid wastewater of these dyes before release into the municipal drain.

Among the numerous dye-wastewater treatment options available, adsorption has been extensively used for its ease of operation, versatility of adsorbents, design simplicity, high efficiency, and comparatively lower cost of operation [3]. Different adsorbents like peanut shell [6], activated carbon [7], zeolites [8], hydrogel beads [9], and biochar [10] have all been explored to remove dyes from aqueous solution, with biochar exhibiting much promise.

Biochar, which is the solid carbonaceous residue from biomass pyrolysis, has received much attention as a promising alternative adsorbent owing to reasons such as abundant surface functional groups, porosity, surface area, and diverse biomass sources [11]. Many biomasses – spent mushroom substrate [12], macroalgae (*Saccharina japonica*) [13,14], palm petiole [15], and sewage sludge [16] – have been explored in biochar production.

Sewage sludge is simply the residue generated from wastewater treatment [17]. Annually, the European Union (EU) and China alone generate over 30 million and 54.8 million tons of sewage sludge (20% solids), respectively [18]. Also, the United States of America (USA) and South Africa (Johannesburg), respectively, generate over 6.2 million metric tons (dry) [19] and 103,295 tons [20] of sewage sludge annually. Unfortunately, the conventional alternative use of sewage sludge is now deemed either unacceptable, per environmental protection legislations, or inadequate in handling the huge waste generation rate [17,18]. Consequently, many studies have now focused on its conversion to biochar for remediation purposes and in environmental management, where a reduction in the volume of the sewage sludge can be achieved in conjunction with the elimination of pathogens [21]. Sewage sludge biochar (SBC) generally contains high ash content and low surface area, if left untreated and/not activated [22]. This may be of concern in applications where high surface area is a requirement. Interestingly, recent research

†To whom correspondence should be addressed.
E-mail: shwoo@hanbat.ac.kr

[23] has found that ash content and functional groups were more important controlling factors in the adsorption of a triarylmethane dye, crystal violet (CV), than surface area. The question thus arises as to whether, by extension, ash content and functional groups of biochar would affect dyes belonging to the same triarylmethane class in the same way or not.

Therefore, in this study, biochar from sewage sludge (SBC), the unintended waste, generated in abundance from wastewater treatment industries with high ash content, was utilized as an adsorbent to study the adsorption behavior/dynamics of two dyes, belonging to the triarylmethane class, CV (triaminotriphenylmethane) and malachite green (MG; diaminotriphenylmethane). Experiments such as adsorbent characterization, the effect of initial solution pH, isotherm studies, kinetics studies, and adsorption mechanism studies were also performed.

MATERIALS AND METHODS

1. Materials and Biochar Preparation

MG, congo red (CR), iron (III) chloride ($FeCl_3 \cdot 6H_2O$, 97.0%), and aluminum sulfate [$Al_2(SO_4)_3 \cdot xH_2O$, 98.0%] were obtained from Sigma Chemical Co. in USA. The CV (Biological stain commission certified), basic blue 41 (BB41), and methylene blue (MB) dyes were purchased from Sigma Chemical Co. in China (refer to Table S1 for the properties of the dyes). Hydrochloric acid (HCl, 35.0-37.0%), sodium hydroxide (NaOH, 98.0%), potassium chloride (KCl, 99.0%), sodium chloride (NaCl, 99.5%), anhydrous magnesium chloride ($MgCl_2$, 98.0%) and anhydrous calcium chloride ($CaCl_2$, 96.0%) were purchased from Samchun Pure Chemicals Co., Ltd., Korea. SBC was received from Pyreg GmbH, Dörth, Germany and was used without further treatments [the sewage sludge sample, obtained from Dörth, Germany, that was used for the biochar production complied with the standards for heavy metals as set in Directive 86/278/EEC (regarding the use of sewage sludge in agriculture [24])] – the biochar production conditions followed that described elsewhere [16]. In brief, dewatered sewage sludge (at 75% dry weight) was fed into a Pyreg P500 pilot-scale, rotary pyrolysis kiln unit (9,000 mm length×3,000 width×5,800 mm height, PYREG GmbH, Dörth, Germany) and pyrolyzed at 600 °C for 20 min. No inert gas was used as flush gas to drive off pyrolytic vapors. The biochar was allowed to gas out for 5 min and was quenched with water to 30% water content.

2. Biochar Characterization Studies

Functional group analysis of SBC, both before and after adsorption of dye, was undertaken by using Fourier transform and infrared (FTIR) Frontier spectrophotometer (Perkin Elmer Model) with attenuated total reflection (ATR) technique in the 4,000-500 cm^{-1} range. The point of zero charge (pH_{pzc}) of SBC was determined following an established methodology (pH drift method) [25]. Scanning electron microscopy (SEM) (Joel Ltd, JSM-6390) coupled with an energy dispersive spectroscopy (EDS) (Oxford, ISIS, USA) was used to obtain the morphology and surface elemental composition of SBC. Characterizations for the total carbon, hydrogen, nitrogen, oxygen, ash contents, conductivity, and surface area were also performed [16]. The content of metallic species (Na, Mg, Al, Si, P, K, Ca, Mn, Fe) was also determined using infrared coupled plasma mass spectrometry (ICP-MS) (Thermo Scientific iCAP RQ, USA).

3. Batch Adsorption Studies of the Triarylmethane Dyes onto SBC

Preliminary experiments with dyes belonging to triarylmethane (MG and CV), thiazine (MB), and azo (BB41 and CR) dye class were first performed in batch mode with SBC to enable the selection of the model dyes for this study based on the class with the highest adsorption values. Consequently, the triarylmethane class of dyes was selected and used for all further adsorption experiments. Approximately ten mg of SBC was measured into a 20 ml borosilicate glass vial containing 10 ml of 500 mg/l of the desired dye (that is, MG or CV). For pH studies, the initial pH of the dye solution was varied from 2 to 10 using either HCl or NaOH. Initial dye concentration studies were performed by varying the initial concentration of the appropriate dye from 5 to 750 mg/l at pH 6.5 for 48 h. Contact time studies were also performed by sampling dyes at regular time intervals from 0 to 48 h, while keeping the initial concentration at 500 mg/l and pH 6.5. All biochar-dye interactions occurred at 150 rpm on a shaking incubator at 30°, after which samples were drawn from the borosilicate glass vials into 1.5 ml microcentrifuge Eppendorf tubes and centrifuged at 1,832×*g* unit for 10 min. The final dye concentration of the dyes was then computed using absorbance data (HACH DR/2500 spectrophotometer, USA) obtained at wavelengths of 620 nm and 590 nm for MG and CV, respectively. All adsorption experiments were performed in three replicates.

The removal performance of SBC on the triarylmethane dyes was assessed via employing the equilibrium adsorptive capacity equation, defined mathematically as:

$$q_e = \frac{(C_0 - C_e) \times V}{W} \quad (1)$$

where q_e (mg/g) is the equilibrium adsorption capacity of SBC; C_0 (mg/l) and C_e (mg/l) are the initial and equilibrium concentration of either MG or CV in the solution, respectively; V (l) is the volume of MG or CV solution; W (g) is the dry weight of SBC.

The leachability of the metals inherent in SBC was also determined to assess both the adsorption mechanism and evaluate the real application potential of SBC. Specifically, experiments were conducted following that outlined for the batch adsorption studies using the same optimum conditions (pH 6.5; initial dye concentration of 500 mg/l; 48 h). An additional leachability experiment using deionized water at the optimum pH of 6.5 was also conducted.

It is likely that some metallic ions may react directly with dyes and not necessarily be involved in adsorption-related removal mechanisms like ion exchanges. To investigate this, additional experiments were conducted to assess the stand-alone contribution of monovalent (Na^+ and K^+), divalent (Ca^{2+} and Mg^{2+}), and trivalent (Fe^{3+} and Al^{3+}) metallic ions on the decolorization of triarylmethane dyes (MG and CV). Solution containing 0.2 mg of the desired metallic ion was prepared and transferred into a 20 ml borosilicate glass vial containing 200 mg/l of either MG or CV solution. Shaking conditions were then carried out as described earlier and the dye removal efficiency, R (%), was determined using Eq. (2).

$$R\,(\%) = \frac{(C_0 - C_e)}{C_0} \times 100\% \quad (2)$$

4. Adsorption Isotherm Models

Four non-linear adsorption isotherm models were used in fitting the adsorption data: Langmuir [26], Freundlich [27], Redlich-Peterson [28], and Dubinin-Radushkevich [29] isotherm models shown in Eqs. (3), (5), (6), and (7)-(9), respectively. In cases where Langmuir model fitted best, Eq. (4) was applied to describe the favorability or otherwise of the adsorption process [30].

$$q_e = \frac{q_m K_L C_e}{1 + K_L C_e} \tag{3}$$

$$R_L = \frac{1}{1 + K_L C_o} \tag{4}$$

$$q_e = K_F C_e^{1/n} \tag{5}$$

$$q_e = \frac{K_{RP} C_e}{1 + a_{RP} C_e^g} \tag{6}$$

$$q_e = q_{DR} e^{-K_{DR}\varepsilon^2} \tag{7}$$

$$\varepsilon = RT \ln\left(1 + \frac{1}{C_e}\right) \tag{8}$$

$$E = \frac{1}{\sqrt{2K_{DR}}} \tag{9}$$

where q_m (mg/g) is the maximum monolayer adsorption capacity of SBC; K_L (l/mg) is the Langmuir constant which is related to the affinity of the adsorbate to the adsorbent; R_L is the separation factor and suggests irreversible (R_L=0), favorable (0<R_L<1), linear (R_L=1) and unfavorable (R_L>1) adsorption; K_F (mg/g)(l/mg)$^{1/n}$ represents the Freundlich constant; 1/n (dimensionless) is the Freundlich intensity parameter and carries the same interpretation as the values for R_L; K_{RP} (l/g) and a_{RP} (mg/l)$^{-g}$ are Redlich-Peterson constants; g (dimensionless) is an exponent that ranges from 0 to 1; q_{DR} (mg/g) is the theoretical isotherm saturation capacity; K_{DR} (mol^2/kJ^2) is a constant related to sorption energy; ε is the Polanyi potential; R (J/mol·K) is the gas constant; T (K) is the temperature and E (kJ/mol) is the mean adsorption energy. Interpretation of the values of E suggests physical adsorption when it is less than 8 kJ/mol and chemical ion exchange within 8-16 kJ/mol [31].

5. Adsorption Kinetic Models

Three kinetic models – Lagergren pseudo-first- [32], and pseudo-second-order kinetic models [33,34], intraparticle diffusion [35], and Boyd's film diffusion [36] rate – were employed in fitting the kinetic data. These are expressed mathematically as Eqs. (10), (11), (12), and (13), (14), respectively.

$$q_t = q_e(1 - e^{-k_1 t}) \tag{10}$$

$$q_t = \frac{q_e^2 k_2 t}{1 + q_e k_2 t} \text{ and } h = k_2 q_e^2 \tag{11}$$

$$q_t = k_p t^{0.5} + C \tag{12}$$

$$F = \frac{q_t}{q_e} = 1 - \frac{6}{\pi^2}\sum_{n=1}^{\infty}\frac{1}{n^2}\exp(-n^2 Bt) \tag{13}$$

$$B = \frac{\pi^2 D_i}{r^2} \tag{14}$$

where q_t (mg/g) and q_e (mg/g) are dye amounts adsorbed at time, t (min) and equilibrium, respectively; k_1 (1/min), k_2 (g/mg min) and k_p (mg/g min$^{0.5}$) are the pseudo-first-order, pseudo-second-order, and intraparticle diffusion rate constants, respectively; h (mg/g min) is the initial adsorption rate; C (mg/g) is the intercept on the y-axis and describes the boundary layer thickness; F (dimensionless) is the fractional approach to equilibrium, and B (1/min) is the rate coefficient; D_i (cm^2/s) is the effective diffusion coefficient of adsorbate on the surface of SBC and r (cm) is the radius of the adsorbent particles (assuming spherical shape).

Due to the complexity of Eq. (13), an approximated form that involved the application of Fourier transform and further integration could be obtained [37]:

$$Bt = \left(\sqrt{\pi} - \sqrt{\pi - \left(\frac{\pi^2 F}{3}\right)}\right)^2 \text{ for } F < 0.85 \tag{15}$$

$$Bt = -0.498 - \ln(1 - F) \text{ for } F > 0.85 \tag{16}$$

By plotting Bt against t, the rate parameter, B, can be obtained. The mass transfer rate is controlled by intraparticle diffusion if the plot passes through the origin and by film-diffusion or chemical reaction if the plot has an intercept [38,39].

The error generated from applying the aforementioned kinetic models was assessed by employing the sum of squared errors (SSE) approach expressed mathematically by Eq. (17) in conjunction with the regression coefficient (R^2).

$$SSE = \sqrt{\frac{\Sigma(q_{e(exp)} - q_{e(cal)})^2}{N}} \tag{17}$$

where $q_{e(exp)}$ (mg/g) and $q_{e(cal)}$ (mg/g) are the experimental and calculated adsorptive capacities, respectively, and N is the number of data points. The appropriateness of fit was evaluated based on higher R^2 but correspondingly lower SSE values [40].

RESULTS AND DISCUSSION

1. Biochar Characterization

The data from the physicochemical analysis of SBC are shown in Table 1. SBC had low total carbon (18.7%) but high ash content (73.3%), consistent with other published data on biochar from sewage sludge [22]. Values of the molar O/C and H/C ratios for SBC were 0.148 and 0.597, respectively, thus stable. Some researchers [41] recommended O/C (hydrophobicity/hydrophilicity) and H/C (aromaticity) values less than 0.4 and 0.6, respectively, to deem biochar as exhibiting long-term stability. High amounts of phosphorus (64.6 g/kg), calcium (57.3 g/kg), iron (44.6 g/kg), aluminum (65.8 g/kg), and lesser amounts of magnesium (13.2 g/kg), potassium (9.93 g/kg), and sodium (1.82 g/kg) were reported in SBC. Similar observations have also been made by other researchers [21]. Sewage sludge is known to contain high amount of phosphorus, which may result from human excreta and/or phosphorus-containing detergents, further concentrated after pyrolysis or incineration [42]. These results suggested that SBC might potentially adsorb cationic dyes more favorably as the presence of the aforementioned ions, particularly calcium, iron, potassium, magnesium, and sodium in biochars are known to contribute to adsorption [10,13,16].

Table 1. Physicochemical properties of sewage sludge biochar

Adsorbent (sewage sludge biochar) properties									
Elemental analysis (wt%)	C	H	O	N	S	O/C[a]	H/C[a]		
	18.7	0.93	3.7	2.1	0.76	0.148	0.597		
Contents of metals (g/kg)	Na	Mg	Al	P	K	Ca	Mn	Fe	Si
	1.82	13.2	65.8	64.6	9.93	57.3	0.927	44.6	10.9
Others	Ash (%)	pH	Surface area (m^2/g)						
	73.3	7.1	25.6						

[a]On mole basis

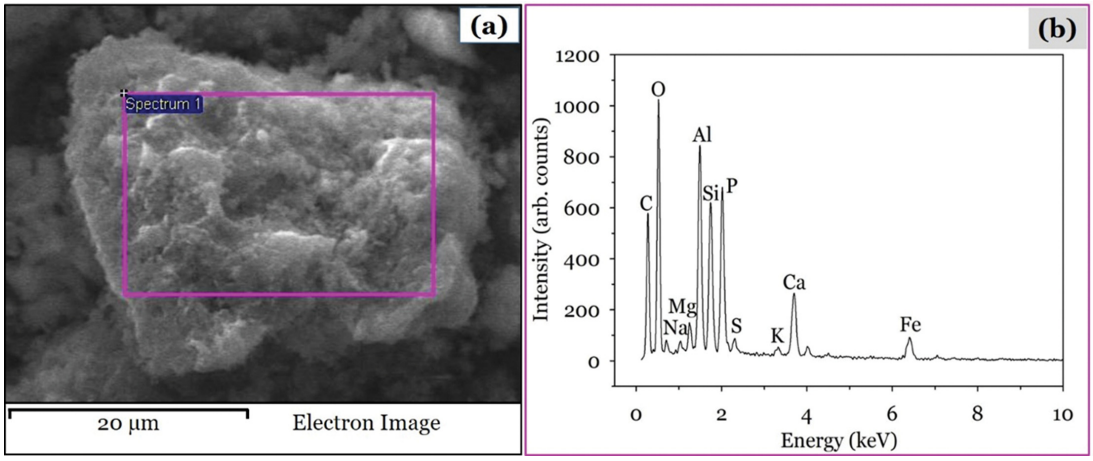

Fig. 1. Image of surface morphology taken with SEM (a) and the corresponding EDS data (b) of sewage sludge biochar.

Fig. 1 shows the image of the surface morphology and the corresponding EDS data of SBC before adsorption experiments. The surface of SBC was rough with no distinct pores, supported by the low surface area of 25.6 m^2/g. Furthermore, the EDS data showed the considerable occurrence of diverse elements including many metals (C, O, Na, Mg, Al, Si, P, S, K, Ca, Fe) on the surface of SBC. These results support the ICP-MS data on the existence of myriads of metals in SBC, therefore buttressing the projected conclusion in the previous paragraph about the potential for heightened ion exchanges.

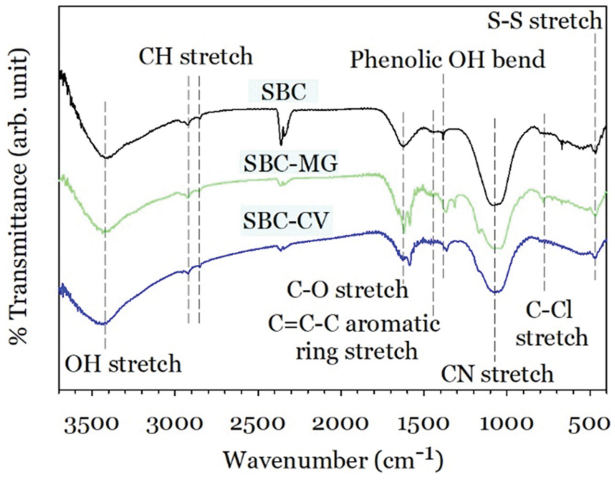

Fig. 2. FTIR data of sewage sludge biochar before (SBC; black) and after adsorption of MG (SBC-MG; green), and CV (SBC-CV; blue).

The description of the functional groups and the assigned wavenumbers from the FTIR spectral data of SBC have been detailed in a previous publication [16]. Prolonged storage of SBC, about 910 days, thus necessitated additional FTIR analysis, which principally revealed some changes to the wavenumbers of the surface functional groups of SBC with the functional groups remaining intact and these are shown in Fig. 2. That is, after the storage, -OH stretching from the hydroxyl groups now occurred at 3,419.5 cm^{-1}. The functional groups of -CH stretching vibrations, C-O stretching of ether, C=C-C stretching of aromatic rings, phenolic OH bend, and disulfide (S-S) stretches, shifted to wavenumbers between 2,922 cm^{-1} and 2,847 cm^{-1}, at 1,632.2 cm^{-1}, 1,455.5 cm^{-1}, 1,386.7 cm^{-1}, and 468.6 cm^{-1}, respectively. Interestingly, an additional peak at 1,070.6 cm^{-1}, assigned to CN stretch was observed on the SBC (probably a consequence of contribution from atmospheric nitrogen due to prolonged storage) [43].

2. Preliminary Adsorption of Dyes from Different Classes by SBC

The results of the preliminary studies employing dyes belonging to different classes (based on the structure) are shown in Fig.

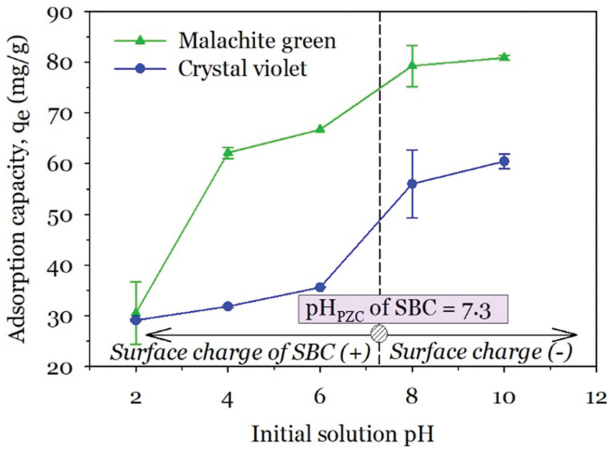

Fig. 3. Effect of initial solution pH on the adsorption of triarylmethane dyes, MG and CV, onto sewage sludge biochar; initial dye concentration, 500 mg/l, 48 h, and 30 °C.

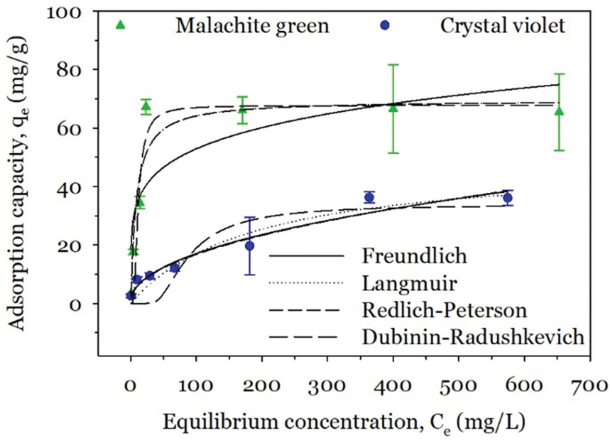

Fig. 4. Adsorption isotherm plots for the adsorption of triarylmethane dyes, MG and CV, onto sewage sludge biochar; pH 6.5, 48 h, and 30 °C.

S1, with Table S1 showing the corresponding dye properties. It is apparent that, the adsorption capacity of SBC for the dyes was charge-dependent; the basic cationic dyes (MG, CV, MB, BB41) were better removed by SBC than the acidic anionic dye, CR. Except for MB, the hierarchy in dye removal followed an order [MG (66.72 mg/g)>BB41 (39.7 mg/g)>CV (35.6 mg/g)>CR (8.29 mg/g)] consistent with the molecular weight of the ionized form of the dyes (Table S1). Among the basic cationic dyes, MB potentially deviated from this trend owing to the larger length of its molecular dimension (1.634 nm×0.793 nm×0.400 nm [44]), Table S1. Also, it is evident that the order of basic, cationic dye removal, according to class generally followed the order: triarylmethane (MG)> azo (BB41)>thiazine (MB), based on the molecular weight of the ionized dye and molecular dimensions as explained above. Based on these findings, the triarylmethane dyes were selected and used as model dyes in subsequent studies.

3. Effect of Initial Solution pH on Adsorption of Triarylmethane Dyes

Fig. 3 shows the effect of initial solution pH on dye adsorption by the SBC. Adsorption of both MG and CV by SBC generally increased with initial solution pH as expected. Both dyes are cationic and thus more H^+ ions arising from decreased pH impaired more dye uptake because of higher competition for adsorption sites and the positive potential on SBC's surface, and vice versa for pH increase. Note that, a sharp increase in q_e of SBC was observed from pH 2 to 4 for only MG. This observation was likely because of the ionized state of MG after pH 2. MG is a diaminotriphenylmethane dye, whereas CV is triaminotriphenylmethane. At very low pH's the amino groups may all become protonated, two- and three-charged amino groups for MG and CV, respectively. Consequently, the repulsion between MG molecules and/ positively charged SBC, as the initial solution pH increases from 2 to 4, will be lesser than it would be for CV, hence the observed result. Another sharp increase in q_e of SBC was observed from pH 6 to 8 for both MG and CV. A plausible reason was the pH_{pzc} of SBC=7.3. As such, SBC had a positive surface charge until the initial solution pH went beyond 7.3, in which case it became negative, which favored cationic dye, MG, and CV adsorption. A pH of 6.5 (corresponding to the pH of deionized water) was selected for subsequent adsorption experiments, considering the issue of cost.

4. Equilibrium Adsorption Isotherms

The plots of the applied adsorption isotherm models are shown in Fig. 4 and the corresponding regression coefficients (R^2) and other relevant parameters in the adsorption models are presented in Table 2. For MG, of the applied isotherm models only Langmuir and Redlich-Peterson models fitted well, based on a high R^2 value of 0.916. Furthermore, the value of the dimensionless factor, g, was unity, and that reduced the Redlich-Peterson isotherm model to that of Langmuir, which was highly indicative of a chemisorption process. The data on CV adsorption by SBC, however, was well fitted by Langmuir (R^2=0.925), Freundlich (R^2=0.954) and Redlich-Peterson (R^2=0.954) isotherm models. The good fit by the

Table 2. Adsorption isotherm parameters for the adsorption of triarylmethane dyes (MG and CV) onto sewage sludge biochars

Dye	Langmuir isotherm					Freundlich isotherm			Redlich-Peterson isotherm				Dubinin-Radushkevich isotherm			
	q_m	K_L	R^2	$R_L{}^a$	$R_L{}^b$	K_F	1/n	R^2	K_{RP}	a_{RP}	g	R^2	q_{RD}	K_{RD}	E	R^2
MG	69.5	0.1200	0.916	0.625	0.011	22.6	0.185	0.719	8.33	0.120	1.00	0.916	67.7	15.70	0.179	0.893
CV	49.0	0.0053	0.925	0.974	0.201	2.02	0.463	0.954	1,780	883	0.54	0.954	33.9	925.8	0.023	0.759

Note: q_m (mg/g), K_L (l/mg), K_F (mg/g)(l/mg)$^{1/n}$, K_{RP} (l/g), a_{RP} (mg/l)$^{-g}$, g (dimensionless), q_{RD} (mg/g), K_{RD} (mol^2/kJ^2) and *E* (kJ/mol)

[a]Initial dye concentration of 5.0 mg/l

[b]Final dye concentration of 750 mg/l

Table 3. Parameters for the applied regression kinetic models for sewage sludge biochar on triarylmethane dyes (MG and CV) removal

Dye	$q_{e(exp)}$ (mg/g)	Pseudo-first-order				Pseudo-second-order				
		$q_{e(cal)}$ (mg/g)	k_1 (l/min)	R^2	SSE	$q_{e(cal)}$ (mg/g)	k_2 (g/mg min)	h (mg/g min)	R^2	SSE
MG	65.9	61.4	0.0259	0.860	3.37	65.2	6.61×10^{-4}	2.810	0.912	2.67
CV	38.3	38.1	0.0092	0.936	2.77	41.2	3.08×10^{-4}	0.523	0.872	3.91

Redlich-Peterson isotherm model is indicative of the involvement of both physisorption and chemisorption in CV adsorption onto SBC. Evidently, the maximum equilibrium adsorption capacity, q_m, of SBC was higher for MG (69.5 mg/g) than for CV (49.0 mg/g). This result was understandable owing to the higher affinity, K_L, of SBC for MG, which was 22.6 times higher than that for CV (K_L=0.0053 l/mg). The above result can be explained. Although both MG and CV are basic triarylmethane dyes, the presence of fewer electronegative atoms (nitrogen) in the chromophore group of MG rendered it more susceptible to attraction by SBC than it was for CV. A similar explanation was offered by [45]; they stated that the order of increasing basicity of elements within the chromophore group of basic, cationic dyes was inversely related to the electronegativity of the cation and that lower electronegativity of the chromophore group may enhance the attractive force to the surface of negatively charged biomass. Dubinin-Radushkevich model had low R^2 values for both MG and CV adsorption, thus indicative of the little role pore-filling played in describing the adsorption process. This result was likely due to the low surface area of SBC (25.6 m^2/g) as pore filling mechanism which normally occurs for microporous adsorbents with high surface area [46], for which SBC is not.

5. Adsorption Kinetic Study

The regression coefficient and all parameters associated with the applied kinetic models in fitting the raw kinetic data for MG and CV adsorption onto SBC are presented in Table 3 and the corresponding plots shown in Fig. 5(a). For MG adsorption, pseudo-second-order model fitted the kinetic data better (higher R^2=0.912; lower SSE=2.67) than the pseudo-first-order model (R^2=0.860; SSE=3.37). The converse held true for CV adsorption where pseudo-first-order model (higher R^2=0.936; lower SSE=2.77) was rather a better fit than the pseudo-second-order model (R^2=0.872; SSE=3.91). Interestingly, although with a higher initial adsorption rate, h, for MG (2.810 mg/g min) than CV uptake (2.810 mg/g min), the latter rather equilibrated faster in 12 h time with the former occurring in 24 h (Fig. 5(a)). Overall, the lower q_m of SBC on CV compared to that of MG suggested that it would likely take less time to reach adsorbate-adsorbent equilibrium or fill the available adsorption sites present for CV adsorption than it would take for MG adsorption.

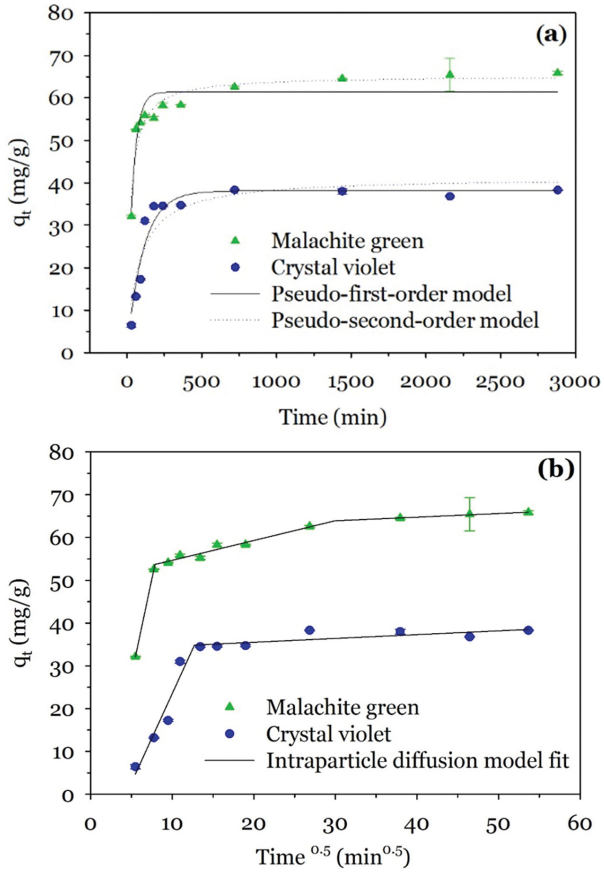

Fig. 5. Pseudo-first- and pseudo-second-order kinetic model plots (a) and intraparticle diffusion plots (b) for the adsorption of triarylmethane dyes, MG and CV, onto sewage sludge biochar; initial dye concentration, 500 mg/l, pH 6.5, and 30 °C.

To understand the mechanism of diffusion of MG and CV into SBC, the intraparticle diffusion model was applied to the kinetic

Table 4. Parameters for the different stages of the intraparticle diffusion model for sewage sludge biochar on triarylmethane dyes (MG and CV) removal

Dye	Stage 1				Stage 2				Stage 3			
	k_p	C	R^2	t_b	k_p	C	R^2	t_b	k_p	C	R^2	t_b
MG	9.043	−17.4	1.000	<61.9	0.463	50.1	0.935	61.9-896	0.085	61.4	0.981	>896
CV	4.163	−18.1	0.896	<162	0.0891	33.8	0.605	>162	n.a.	n.a.	n.a.	n.a.

Note: k_p (mg/g min$^{0.5}$); t_b (min): breakpoint or transition times between the different diffusion stages; n.a.: not applicable.

data, with the results shown graphically in Fig. 5(b) and the associated parameters tabulated in Table 4. The criteria for selecting the number of transition stages was based on both statistical and graphical approaches as proposed in [38]. Multi-linearity was observed for both triarylmethane dyes but with MG showcasing three distinct diffusion stages, whereas CV exhibited two diffusion stages. These stages corresponded to the diffusion of dyes in pores of successively smaller sizes as proposed in [47]. The reasons are likely due to the molecular dimensions and affinity of MG and CV to SBC. The former is less likely as both MG (1.0 nm×1.1 nm×1.2 nm) [48] and CV (0.87 nm×1.025 nm×1.137 nm) [49] have comparable molecular dimensions. On the latter, however, less affinity of CV for SBC, owing to its higher electronegativity, lessened its accessibility to smaller pores of SBC under greater repulsions with narrowing pore size. The transition time between the first and second diffusion stage and the second and third diffusion stage occurred at 61.9 min and 896 min, respectively, for MG adsorption. For CV adsorption, however, it occurred at 162 min. The values of C for adsorption of MG and CV were non-zero, which suggested that intraparticle diffusion was not the sole rate-determining step in controlling the adsorption of both MG and CV from aqueous solution and that other mechanisms such as film diffusion were at play. The parameters from Boyd's film diffusion model employed in determining the diffusion mechanism are shown in Table S2 (Figure not shown). The effective diffusion coefficient of MG (2.63×10^{-9} cm^2/s) was over twice that of CV (1.21×10^{-9} cm^2/s). Besides, the film diffusion model yielded non-zero intercepts (MG=−0.548; CV=−0.560), indicative of the fact that film diffusion or chemical reaction was the rate-determining step [38], which supported the conclusion deduced from the application of the intraparticle diffusion model.

6. Adsorption Mechanism

To elucidate the adsorption mechanism, the FTIR spectra of SBC, post-adsorption of MG, and CV were taken (Fig. 2). The results revealed that similar interactions might have been at play for both MG and CV adsorption. One such interaction was likely hydrogen bonding; incremental shifts in -OH group wavenumber on SBC from 3,419.5 cm^{-1} to 3,430.1 cm^{-1} and 3,445.9 cm^{-1} after MG and CV adsorption, respectively [50]. In addition, the phenolic -OH group shifted to 1,369.5 cm^{-1} (MG adsorption) and 1,366.2 cm^{-1} (CV adsorption) from 1,386.7 cm^{-1}, which further solidifies the potential role of hydrogen bonding for both MG and CV adsorption. Also, shifts in aromatic C=C-C on the SBC from 1,455.5 cm^{-1} to 1,586.0 cm^{-1} and 1,589.3 cm^{-1} for MG and CV, respectively, indicated the likely existence of π-π interactions in describing the adsorption process [46]. Electrostatic interactions also played a minimal role in the adsorption process; adsorption experiments occurred at pH 6.5 although the pH_{pzc} of SBC was 7.3 (discussed under section 3). Pore filling may have also played a minimal role (discussed under section 4) for both MG and CV adsorption.

To also analyze the contribution of ion exchange on MG and CV dye adsorption by SBC, leaching experiments with deionized water, MG, and CV were performed and the results of the metal content of the leachates, post adsorption are shown in Table 5. The results show a strong dependency of type and quantity of leached ions on the adsorbate type employed; the total quantity of leached ions was over twice for MG (70.6 mg/kg) than it was for CV (34.9 mg/kg). Interestingly, using the control leachate (SBC in deionized water) as the reference – Na (2.6 mg/kg), Mg (1.06 mg/kg), Al (0.03 mg/kg), Si (0.98 mg/kg), P (1.50 mg/kg), K (0.82 mg/kg), Ca (4.70 mg/kg), Mn (0.01 mg/kg), and Fe (null) – the quantity of each ion type leached increased by a larger factor for MG than for CV except for Na. Based on the quantity of additional ions leached into the adsorbate solution from SBC, the dominant ions involved in ion exchange with MG were P (16.7 mg/kg), Al (10.3 mg/kg), Ca (9.81 mg/kg), and K (6.23 mg/kg). For CV, the dominant ion exchange species were Na (7.67 mg/kg), K (5.40 mg/kg), and Ca (6.876 mg/kg). Interestingly, all other ions present in SBC played some role in ion exchanges with both MG and CV except for Fe, which was not involved in ion exchange with either MG or CV, based on null values in leachate which suggested no ion release from SBC. A similar observation of no involvement in ion exchange with CV was also seen for Al. Reports of higher leached quantities of ions such as Na, K, Mg, and Ca in sewage sludge biochar do exist in the literature [51]. The dependency of the type and quantity of leach-

Table 5. Concentration of metals in the leachate derived from deionized water, malachite green, and crystal violet, post-adsorption with sewage sludge biochar

Metal	Concentration in leachate (mg/kg)		
	Deionized water	Malachite green	Crystal violet
Na	2.600	5.768	10.27
Mg	1.058	3.846	1.485
Al	0.025	10.28	0.006
Si	0.983	3.761	2.439
P	1.497	18.20	2.586
K	0.821	7.055	6.224
Ca	4.700	14.51	6.876
Mn	0.006	0.278	0.012
Fe	0.000	0.129	0.000

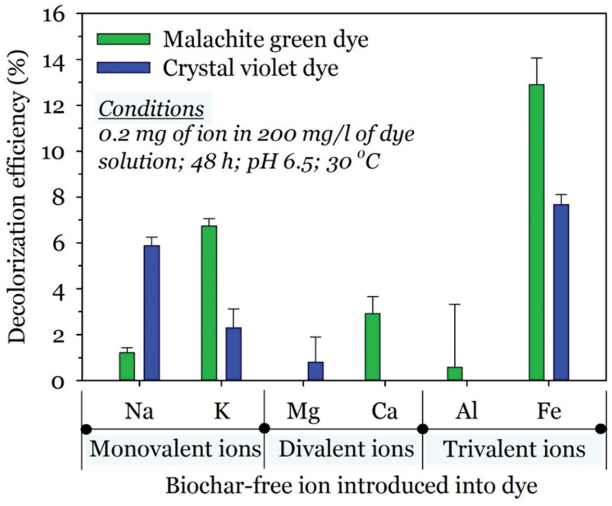

Fig. 6. Stand-alone contributions of free metallic ions on the decolorization of triarylmethane dyes, MG and CV.

able metallic ions from SBC on the type of adsorbate employed was also indicative of the fact that the type of metallic species present in the biochar was rather more deterministic of the outcome of adsorption than just ash content in terms of removal performance for triarylmethane dyes.

It is likely that some metallic ions may react directly with dyes and not necessarily be involved in adsorption-related removal mechanisms like ion exchange. As such, a biochar-free process, where only the metallic ion is introduced into the dye solution, was undertaken. Fig. 6, therefore, shows the stand-alone contribution of monovalent (Na^+ and K^+), divalent (Ca^{2+} and Mg^{2+}), and trivalent (Fe^{3+} and Al^{3+}) metallic ions on the decolorization of triarylmethane dyes (MG and CV). Interestingly, although minimal, both MG and CV underwent some decolorization in the presence of free metallic ions in the respective dye solution. MG and CV were most sensitive to the presence of Fe (respectively, 13% and 7.7%) in solution, followed by K (6.7%), Ca (2.9%) and Na (1.2%) for MG and Na (5.9%), K (2.3%), and Mg (0.8%) for CV. According to [52], $FeCl_3$ has been used as a coagulating agent for dye removal in industrial setups. It is thus suggested that the higher MG and CV removal with Fe may have been due to micro-aggregation of dyes, which could have settled during the centrifugation stage before spectrophotometric readings. Furthermore, there was no clear trend on dye decolorization based on the valency of the metallic ions used. The results show that some adsorption-unrelated chemical reactions may have also been involved in MG and CV decolorization. More investigations are needed in the future to reveal what these underlying reactions might be.

7. Comparison with other Carbonaceous Adsorbents in Literature

Table 6 presents a comparison of the maximum adsorption capacity values of various carbonaceous adsorbents in the literature to that in this study. For MG, adsorption, all adsorbents performed better than SBC (69.5 mg/g) except for activated carbon from *Racinus communis* (27.78 mg/g) [53] and rice husk biochar (67.6 mg/g) [54], which performed poorly. Despite the better surface area and adsorption performance, all these adsorbents utilized more production steps – from activation [53,55-57] and liquefaction [54] – and/consumed more energy [higher pyrolysis temperature and pyrolysis time; 800 °C and 1.5 h ([58])].

For CV adsorption, except for *Racinus communis* pericarp carbon [59], all adsorbents tabulated in Table 6 outperformed SBC in terms of maximum adsorption capacity. However, SBC performed comparatively (49.0 mg/g) with *Racinus communis* pericarp carbon (48.0 mg/g) [59], even with a surface area 19.3-times smaller than that of *Racinus communis* pericarp carbon (495 m^2/g). Besides, compared to SBC production, all adsorbents, except for Korean cabbage biochar [23], required numerous preparation steps [23,58-60] and steam injection (for gasification [61]), which likely render them more costly. Consequently, more studies are required to enhance the adsorption capacity of SBC.

CONCLUSIONS

The adsorption behavior of MG and CV by SBC was more similar than dissimilar; both physisorption and chemisorption were involved as well as the existence of similar adsorption mechanisms. Higher uptake of MG (69.5 mg/g) than CV (49.0 mg/g) by SBC was indicative of the roles that molecular size and electronegativity of the ionized form of the dyes and sensitivity to different ions (P, Al, K, Ca, Mg, etc.) present in the biochar, played in dye decolorization. The dependency of the type and quantity of leachable metallic ions from SBC on the type of adsorbate employed indicated that the type of metallic ions present in the biochar was rather more deterministic of the outcome of adsorption by ion exchange than just ash content for triarylmethane dyes.

SUPPORTING INFORMATION

Additional information as noted in the text. This information is available via the Internet at http://www.springer.com/chemistry/journal/11814.

Table 6. Comparison of the Langmuir maximum monolayer adsorption capacity of SBC to other carbonaceous adsorbents in the literature

Dye	Adsorbent	Surface area (m^2/g)	Temp. (°C)/time	q_m (mg/g)	Reference
MG	*Racinus communis* activated carbon	n.r	n.r.	27.78	[53]
	Rice husk biochar (ethanol liquefaction)	9.2	260/20 min	67.6	[54]
	Cattail activated carbon	441	850/2 h	210.2	[55]
	Tea leaves activated carbon	134	450/1 h	256.4	[56]
	NaOH-activated biochar	32.1	500/1 h	1,341	[57]
	Wheat straw-fed mealworm frass biochar	238.4	800/1.5 h	1,738.6	[58]
	SBC	25.6	600/20 min	69.5	This study
CV	*Racinus communis* pericarp carbon	495	n.r.	48.0	[59]
	Tomato paste waste nanoporous carbon	722	500/1 h	68.97	[60]
	Wheat straw-fed mealworm frass biochar	238.4	800/1.5 h	175.6	[58]
	Lignite activated carbon	723	n.r.	271.0	[23]
	Municipal solid waste char*	11.4	n.r.	356	[61]
	Korean cabbage waste	11.4	500/1 h	1,304	[23]
	SBC	25.6	600/20 min	49.0	This study

*Gasification process and not strict pyrolysis; n.r.: not reported

REFERENCES

1. V. Katheresan, J. Kansedo and S. Y. Lau, *J. Environ. Chem. Eng.*, **6**, 4676 (2018).
2. M. T. Yagub, T. K. Sen, S. Afroze and H. M. Ang, *Adv. Colloid Interface Sci.*, **209**, 172 (2014).
3. T. Robinson, G. McMullan, R. Marchant and P. Nigam, *Bioresour. Technol.*, **77**, 247 (2001).
4. C. J. Ogugbue and T. Sawidis, *Biotechnol. Res. Int.*, **2011**, 1 (2011).
5. V. Gupta, I. Ali and D. Mohan, *J. Colloid Interface Sci.*, **265**, 257 (2003).
6. J. Liu, Z. Wang, H. Li, C. Hu, P. Raymer and Q. Huang, *Bioresour. Technol.*, **249**, 307 (2018).
7. P. S. Kumar, S. J. Varjani and S. Suganya, *Bioresour. Technol.*, **250**, 716 (2018).
8. N. M. Mahmoodi and M. H. Saffar-Dastgerdi, *Microchem. J.*, **145**, 74 (2019).
9. G. Ohemeng-Boahen, D. D. Sewu and S. H. Woo, *Environ. Sci. Pollut. Res.*, **26**, 33030 (2019).
10. D. D. Sewu, P. Boakye, H. Jung and S. H. Woo, *Bioresour. Technol.*, **244**, 1142 (2017).
11. D. Mohan, A. Sarswat, Y. S. Ok and C. U. Pittman Jr., *Bioresour. Technol.*, **160**, 191 (2014).
12. D. D. Sewu, H. Jung, S. S. Kim, D. S. Lee and S. H. Woo, *Bioresour. Technol.*, **277**, 77 (2019).
13. P. Boakye, H. N. Tran, D. S. Lee and S. H. Woo, *J. Environ. Manage.*, **233**, 165 (2019).
14. D. D. Sewu, D. S. Lee, H. N. Tran and S. H. Woo, *J. Taiwan Inst. Chem. E.*, **104**, 106 (2019).
15. H.-O. Chahinez, O. Abdelkader, Y. Leila and H. N. Tran, *Environ. Technol. Inno.*, **19**, 100872 (2020).
16. D. Kalderis, B. Kayan, S. Akay, E. Kulaksız and B. Gözmen, *J. Environ. Chem. Eng.*, **5**, 2222 (2017).
17. K. Smith, G. Fowler, S. Pullket and N. J. D. Graham, *Water Res.*, **43**, 2569 (2009).
18. B. Xiao, Q. Dai, X. Yu, P. Yu, S. Zhai, R. Liu, X. Guo and H. Chen, *J. Hazard. Mater.*, **343**, 347 (2018).
19. P. Oleszczuk, S. E. Hale, J. Lehmann and G. Cornelissen, *Bioresour. Technol.*, **111**, 84 (2012).
20. N. C. Shiba and F. Ntuli, *Waste Manage.*, **60**, 191 (2017).
21. K. Phoungthong, H. Zhang, L.-M. Shao and P.-J. He, *J. Mater. Cycles Waste Manage.*, **20**, 2089 (2018).
22. L. Leng, X. Yuan, H. Huang, J. Shao, H. Wang, X. Chen and G. Zeng, *Appl. Surf. Sci.*, **346**, 223 (2015).
23. D. D. Sewu, P. Boakye and S. H. Woo, *Bioresour. Technol.*, **224**, 206 (2017).
24. E. Commission, *Offic. J. Eur. Comm.*, **181**, 6 (1986).
25. G. Newcombe, R. Hayes and M. Drikas, *Colloids Surf. A*, **78**, 65 (1993).
26. I. Langmuir, *J. Am. Chem. Soc.*, **38**, 2221 (1916).
27. L. Yao, J. Yang, P. Zhang and L. Deng, *Bioresour. Technol.*, **256**, 208 (2018).
28. H. N. Tran, S.-J. You, A. Hosseini-Bandegharaei and H.-P. Chao, *Water Res.*, **120**, 88 (2017).
29. M. Dubinin, *Chem. Rev.*, **60**, 235 (1960).
30. T. W. Weber and R. K. Chakravorti, *AIChE J.*, **20**, 228 (1974).
31. S. K. Low and M. C. Tan, *J. Environ. Chem. Eng.*, **6**, 3502 (2018).
32. S. Lagergren, *Sven Vetenskapsakad. Handingarl*, **24**, 1 (1898).
33. G. Blanchard, M. Maunaye and G. Martin, *Water Res.*, **18**, 1501 (1984).
34. Y. S. Ho, D. J. Wase and C. Forster, *Environ. Technol.*, **17**, 71 (1996).
35. W. J. Weber and J. C. Morris, *J. Sanit. Eng. Div., Am. Soc. Civ. Eng.*, **89**, 31 (1963).
36. G. Boyd, A. Adamson and L. Myers Jr., *J. Am. Chem. Soc.*, **69**, 2836 (1947).
37. D. Reichenberg, *J. Am. Chem. Soc.*, **75**, 589 (1953).
38. G. F. Malash and M. I. El-Khaiary, *Chem. Eng. J.*, **163**, 256 (2010).
39. C. Yao and T. Chen, *Chem. Eng. Res. Des.*, **119**, 87 (2017).
40. I. Tan, B. Hameed and A. Ahmad, *Chem. Eng. J.*, **127**, 111 (2007).
41. S. Schimmelpfennig and B. Glaser, *J. Environ. Qual.*, **41**, 1001 (2012).
42. O. Krüger, A. Grabner and C. Adam, *Environ. Sci. Technol.*, **48**, 11811 (2014).
43. J. Coates, in *Encyclopedia of analytical chemistry: Applications, Theory and instrumentation*, R. A. Meyers Ed., John Wiley and Sons Ltd, Chichester (2000).
44. X. Zhao, X. Bu, T. Wu, S.-T. Zheng, L. Wang and P. Feng, *Nat. Commun.*, **4**, 1 (2013).
45. R. Tabaraki and N. Sadeghinejad, *Water Sci. Technol.*, **75**, 2631 (2017).
46. H. N. Tran, S.-J. You and H.-P. Chao, *Korean J. Chem. Eng.*, **34**, 1708 (2017).
47. Y. Ho and G. McKay, *Can. J. Chem. Eng.*, **76**, 822 (1998).
48. E. Castellini, R. Andreoli, G. Malavasi and A. Pedone, *Colloids Surf. A.*, **329**, 31 (2008).
49. A. R. Abbasi, M. Karimi and K. Daasbjerg, *Ultrason. Sonochem.*, **37**, 182 (2017).
50. A. Wathukarage, I. Herath, M. Iqbal and M. Vithanage, *Environ. Geochem. Health*, **41**, 1647 (2019).
51. X. Chen, L. Yang, S. C. Myneni and Y. Deng, *Chem. Eng. J.*, **373**, 840 (2019).
52. K. Singh and S. Arora, *Crit. Rev. Environ. Sci. Technol.*, **41**, 807 (2011).
53. T. Santhi, S. Manonmani and T. Smitha, *J. Hazard. Mater.*, **179**, 178 (2010).
54. L. Leng, X. Yuan, G. Zeng, J. Shao, X. Chen, Z. Wu, H. Wang and X. Peng, *Fuel*, **155**, 77 (2015).
55. M. Yu, Y. Han, J. Li and L. Wang, *Chem. Eng. J.*, **317**, 493 (2017).
56. E. Akar, A. Altinişik and Y. Seki, *Ecol. Eng.*, **52**, 19 (2013).
57. M. Choudhary, R. Kumar and S. Neogi, *J. Hazard. Mater.*, **392**, 122441 (2020).
58. S.-S. Yang, J.-H. Kang, T.-R. Xie, L. He, D.-F. Xing, N.-Q. Ren, S.-H. Ho and W.-M. Wu, *J. Cleaner Prod.*, **227**, 33 (2019).
59. S. Madhavakrishnan, K. Manickavasagam, R. Vasanthakumar, K. Rasappan, R. Mohanraj and S. Pattabhi, *E-J. Chem.*, **6**, 1109 (2009).
60. F. Güzel, H. Sayğılı, G. A. Sayğılı and F. Koyuncu, *J. Ind. Eng. Chem.*, **20**, 3375 (2014).
61. H. Jung, D. D. Sewu, G. Ohemeng-Boahen, D. S. Lee and S. H. Woo, *Waste Manage.*, **91**, 33 (2019).

Supporting Information

Decolorization of triarylmethane dyes, malachite green, and crystal violet, by sewage sludge biochar: Isotherm, kinetics, and adsorption mechanism comparison

Divine Damertey Sewu[*,], Dae Sung Lee[***], Seung Han Woo[*,**,†], and Dimitrios Kalderis[****]**

*Life Green Technology Co. Ltd., 875 Yuseong-daero, Yuseong-gu, Daejeon 34158, Korea
**Department of Chemical and Biological Engineering, Hanbat National University,
125 Dongseo-daero, Yuseong-gu, Daejeon 34158, Korea
***Department of Environmental Engineering, Kyungpook National University, 80 Daehak-ro, Buk-gu, Daegu 41566, Korea
****Department of Electronics Engineering, School of Engineering, Hellenic Mediterranean University, Chania, Crete, Greece
(*Received 8 September 2020 • Revised 24 November 2020 • Accepted 11 December 2020*)

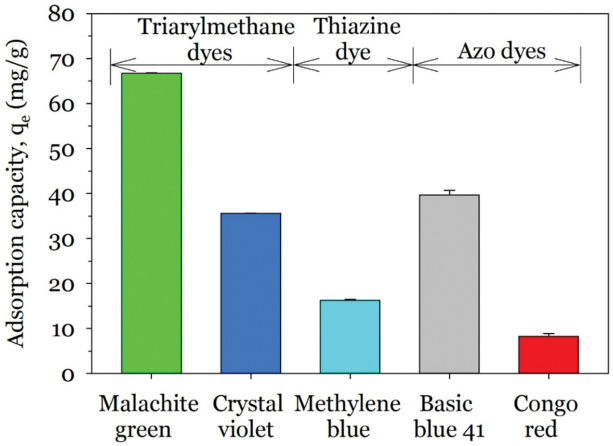

Fig. S1. Preliminary studies on the adsorption of dyes of different classes by high-ash laden sewage sludge biochar; initial dye concentration, 500 mg/l, 48 h, 30 °C.

Table S1. Characteristics of dyes used in the preliminary studies for the selection of the model dye class

Dye	Class	Charge	Molecular weight (g/mol)	Dimensions (nm)[b]
Malachite green oxalate	Triarylmethane	Cationic	463.50 (364.9)[a]	1.20×1.10×1.00 [1]
Crystal violet	Triarylmethane	Cationic	407.99 (372.5)[a]	1.137×1.025×0.87 [2]
Methylene blue	Thiazine	Cationic	319.85 (284.4)[a]	1.634×0.793×0.400 [3]
Basic blue 41	Mono azo	Cationic	482.57 (371.0)[a]	n.a.
Congo red	Diazo	Anionic	696.66 (650.7)[a]	2.62×0.74×0.43 [4]

Note: n.a.: not available; [a]: Molecular weight in ionized form [5]; [b]: Dimensions are in length×width×depth.

Table S2. The parameters of the Boyd's film diffusion rate model in the first stage of adsorption

Dye	B (1/min)	C	R^2	t_b (min)	D_i (cm^2/s)
Malachite green	0.0277	−0.548	1.000	64.63	2.63×10^{-9}
Crystal violet	0.0128	−0.560	0.911	183.9	1.21×10^{-9}

Note: B: film diffusion rate constant; D_i: effective diffusion coefficient of adsorbate on the surface of SBC; t_b: breakpoint or transition times between the different diffusion stages.

REFERENCES

1. E. Castellini, R. Andreoli, G. Malavasi and A. Pedone, *Colloids Surf.* A., **329**, 31 (2008).
2. A. R. Abbasi, M. Karimi and K. Daasbjerg, *Ultrason. Sonochem*., **37**, 182 (2017).
3. X. Zhao, X. Bu, T. Wu, S.-T. Zheng, L. Wang and P. Feng, *Nat. Commun*., **4**, 1 (2013).
4. C. Pelekani and V. L. Snoeyink, *Carbon*, **39**, 25 (2001).
5. K. Sharma, A. K. Dalai and R. K. Vyas, *Rev. Chem. Eng*., **34**, 107 (2017).